Articles

Secondary Interactions Significantly Removed from the Sulfonamide Binding Pocket of Carbonic Anhydrase II Influence Inhibitor Binding Constants

P. Ann Boriack and David W. Christianson*

Department of Chemistry, University of Pennsylvania, Philadelphia, Pennsylvania 19104-6323

Jill Kingery-Wood[†] and George M. Whitesides*

Department of Chemistry, Harvard University, Cambridge, Massachusetts 02138

Received January 12, 1995[®]

A series of competitive inhibitors of carbonic anhydrase II (CAII; EC 4.2.1.1) that consists of oligo(ethylene glycol) units attached to *p*-benzenesulfonamides with pendant amino acids, $H_2NSO_2C_6H_4CONHCH_2CH_2OCH_2CH_2OCH_2CH_2NHCOCHRNH_3^+$, have been synthesized and examined using competitive fluorescence assays. Three of the strongest inhibitors, designated $EG_3NH_3^+$, $EG_3GlyNH_3^+$, and $EG_3PheNH_3^+$, have been studied by X-ray crystallographic methods at limiting resolutions of 1.9, 2.0, and 2.3 Å, respectively. The sulfonamide–zinc binding modes and the association of the ethylene glycol linkers to the hydrophobic patch of the active site are similar in all three inhibitors. Differences in the values of K_d are therefore not due to differences in zinc coordination or to differences in the modes of enzyme–glycol association but instead appear to arise from interaction of the pendant amino acids with the surface of the protein. These pendent groups are, however, not sufficiently ordered to be visible in electron density maps. Thus, structural variations of inhibitors at locations distant from the primary binding (i.e., the sulfonamide group) site affect the overall binding affinities of inhibitors (e.g., K_d ($EG_3PheNH_3^+$) = 14 nM as compared with K_d ($EG_3GluNH_3^+$) = 100 nM).

Introduction

Human carbonic anhydrase II (CAII; EC 4.2.1.1) is a metalloenzyme of 260 amino acids that contains one catalytically obligatory zinc ion. The conical active site cavity of the enzyme is approximately 15 Å deep and is comprised of a hydrophobic region and a hydrophilic region. Zinc is liganded by three histidine residues located at the bottom of the active site cavity; the role of this metal ion is to supply nucleophilic, zinc-bound hydroxide ion for the catalytic hydration of carbon dioxide.[1–4]

Seven known isozymes of carbonic anhydrase are found *in vivo*, but the most immediate pharmaceutical relevance of CAII is in glaucoma pathology: CAII-catalyzed bicarbonate production in the aqueous humor is linked to elevated intraocular pressure;[5,6] since aryl sulfonamides are inhibitors of CAII, they are effective in the regulation of intraocular pressure and are therefore potentially useful in the treatment of glaucoma.[7–13] The 2.0 and 1.54 Å resolution crystal structures of CAII[14–16] as well as the structures of CAII complexed with sulfonamide inhibitors[14–15,17–21] make this enzyme an attractive target for testing strategies in structure-based drug design.

Here, we describe a part of our continuing studies of enzyme–inhibitor interactions using CAII and derivatives of benzenesulfonamide as a model system. We are interested in exploring the factors associated with enhanced binding of inhibitors to the enzyme at locations other than the primary binding site. Using a known inhibitor (P), we add appropriate secondary
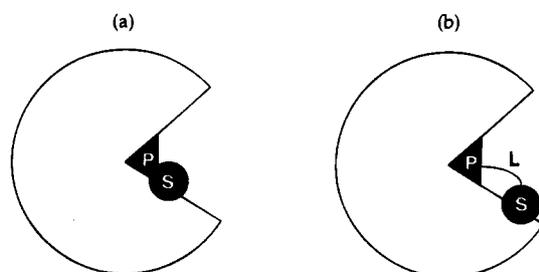

Figure 1. (a) Carbonic anhydrase with adjacent primary and secondary binding sites. (b) Carbonic anhydrase with remote primary and secondary binding sites.

groups (S) that appear capable of interacting with the surface of the enzyme at a site adjacent to the primary binding site. Depending on the location of the secondary site, the two groups P and S may be joined by a linker L (Figure 1).

Previously, we looked at two types of molecular linkers—one based on repeating glycine units (Gly_n) and the other based on repeating ethylene glycol units (EG_n) attached to *p*-benzenesulfonamides—to probe the region flanking the enzyme active site.[22] Crystal structures were obtained for several complexes of CAII with inhibitors bearing a Gly_n terminal chain,[21] and inhibition constants (K_d) were measured for both series.[22] In the EG_n series, K_d increased only very slightly for $n = 1–5$, despite the fact that the "inner" $(EG)_n$ moieties ($n = 1–3$) interacted sufficiently with the protein to influence proton relaxation times. The relatively modest variation of K_d with n may be due to a fortuitous cancellation of changes in ΔH and $T\Delta S$, although the independence of ΔG for the binding of both $(Gly)_n$ and $(EG)_n$ benzenesulfonamide derivatives with chain length n strains coincidence.

[†] Current address: Miles Inc., 400 Morgan Lane, West Haven, CT 06516-4175.
[®] Abstract published in *Advance ACS Abstracts,* June 1, 1995.

Scheme 1
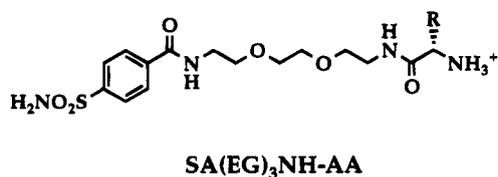
SA(EG)₃NH-AA

Table 1. CAII–SA(EG)₃NH–AA Binding Affinities

AA	compd	K_d (nM)	AA	compd	K_d (nM)
Phe	1	14	Ser	5	41
Gly	2	19	Lys	6	50
H	3	43	Glu	7	100
Leu	4	16			

In order to explore possible secondary binding sites for amino acids in the CAII active site, we have attached pendant amino acids to an arylsulfonamide–EG₃ moiety (Scheme 1). These studies were intended to complement similar studies in which the structural variation was achieved closer to the aryl group.[22] Our objective was to determine whether secondary binding interactions far from the primary binding site could influence K_d.

Results

The inhibitors were screened using a competitive fluorescence assay with dansylamide[22,23] to see if charge, polarity, or hydrophobicity would enhance the binding of the sulfonamide (Table 1). The range of binding constants was approximately a factor of 7. The charged amino acid derivatives (lysine and glutamate) bound less tightly than inhibitors bearing neutral polar groups (serine); inhibitors with the nonpolar amino acids Phe, Leu, and Gly bound to the enzyme with the greatest affinity. These results prompted us to explore the hydrophobic EG₃PheNH₃⁺ (**1**) and EG₃GlyNH₃⁺ (**2**) derivatives (and EG₃NH₃⁺ (**3**) as a control) by X-ray crystallographic methods.

The crystal structures of CAII–inhibitor complexes reveal that the overall structure of CAII remains essentially unchanged upon the binding of each inhibitor. Most differences between the structures of the native and inhibitor-complexed enzymes result from conformational changes of occasional surface residues. As noted in the Experimental Section, difference electron density maps of all three enzyme–inhibitor complexes reveal poor or completely lacking electron density for the terminal glycol residue of each inhibitor (regardless of whether or not an amino acid is attached). If the interactions between each inhibitor and the enzyme active site were insufficient to anchor the terminus of the glycol linker in a single conformation, the resulting molecular disorder of the linker would account for the lack of interpretable electron density. Weak interactions in several conformations, or differences in the entropy of interaction between ligand and protein, could still produce significant differences in K_d. Electron density maps of the complexes of CAII with EG₃PheNH₃⁺, EG₃GlyNH₃⁺, and EG₃NH₃⁺ are found in Figures 2, 3, and 4, respectively.

The sulfonamide–zinc binding mode of each inhibitor is in accord with the binding of other sulfonamides to CAII.[17–21] In each CAII–sulfonamide complex, the ionized sulfonamide nitrogen displaces zinc-bound hydroxide such that tetrahedral metal coordination is maintained. The zinc-bound sulfonamide nitrogen also donates a hydrogen bond to the hydroxyl group of

Table 2. Selected Carbonic Anhydrase II–Inhibitor Interactions

inhibitor atom	enzyme residue	separation (Å)ᵃ EG₃-PheNH₃⁺	EG₃-GlyNH₃⁺	EG₃-NH₃⁺
sulfonamide N1	Zn²⁺	2.2	2.2	2.3
	Thr(199) Oγ	2.9*	2.8*	2.7*
sulfonamide O1	Thr(199) NH	3.1*	2.9*	2.9*
sulfonamide O2	Zn²⁺	3.1	3.2	3.1
C=O	H₂O (425)		2.6*	2.9*
NH	H₂O (423)		2.8*	

ᵃ An asterisk (*) denotes a possible hydrogen bond, as judged from distance and stereochemical criteria.

Thr199, which in turn donates a hydrogen bond to the ionized carboxylate of Glu106. One of the sulfonamide oxygen atoms displaces the so-called "deep" water molecule found at the mouth of the hydrophobic pocket in the native enzyme.[14,15] Selected distances of enzyme–inhibitor interactions are given in Table 2.

The crystallographically-visible portion of the EG₃ tail of each inhibitor packs against a hydrophobic wall comprised of Pro201, Pro202, and Leu198. This interaction minimizes the solvent-accessible surface area of each hydrophobic glycol group; it is apparently more energetically favorable than any possible hydrogen bonds that glycol oxygen atoms might exploit in the hydrophilic half of the active site cleft. An alternate conformation of the EG₃NH₃⁺ tail (<25% occupancy) may, however, result in a hydrogen bond between the side chain amide nitrogen of Gln92 and an oxygen atom of the glycol tail. We cannot unambiguously identify this interaction as important, however, since the electron density map of the CAII–EG₃NH₃⁺ complex is rather noisy (Figure 4). Not surprisingly, the exact conformation of each glycol tail differs only slightly among the three inhibitors (Figure 5).

The arylsulfonamide anchoring groups of each inhibitor are essentially superimposable in their enzyme-bound conformation (Figure 5). The amide nitrogen linking the arylsulfonamide and the glycol tails of both EG₃GlyNH₃⁺ and EG₃NH₃⁺ donates a hydrogen bond to a solvent molecule, which in turn donates a hydrogen bond to the backbone carbonyl oxygen of Pro201. In addition, the carbonyl oxygen of EG₃GlyNH₃⁺ accepts a hydrogen bond from a water molecule, which in turn accepts a hydrogen bond from the side chain amide nitrogen of Gln92. Electron density corresponding to the solvent molecule bridging the inhibitor and Gln92 is obscured by the alternate conformation of the glycol tail in the EG₃NH₃⁺ complex. Although it is difficult to determine the extent to which these inhibitor–solvent–protein hydrogen bond networks contribute to enzyme–inhibitor affinity, it is satisfying that the hydrogen bond directionality of these networks can be established unambiguously from crystal structures. A scheme of the CAII–EG₃GlyNH₃⁺ binding mode is found in Figure 6.

No water-mediated hydrogen bonds are observed between the protein and the bound inhibitor in the complex of CAII with EG₃PheNH₃⁺ (Figure 2). This observation may be an artifact of the relatively low resolution (2.3 Å) of this structure. We note that weak electron density is observed in the locations of molecules bridging the enzyme and its bound inhibitor; since the refined thermal B factors of water molecules modeled into this density were greater than 50 Å², however, they were not included in the final set of atomic coordinates.
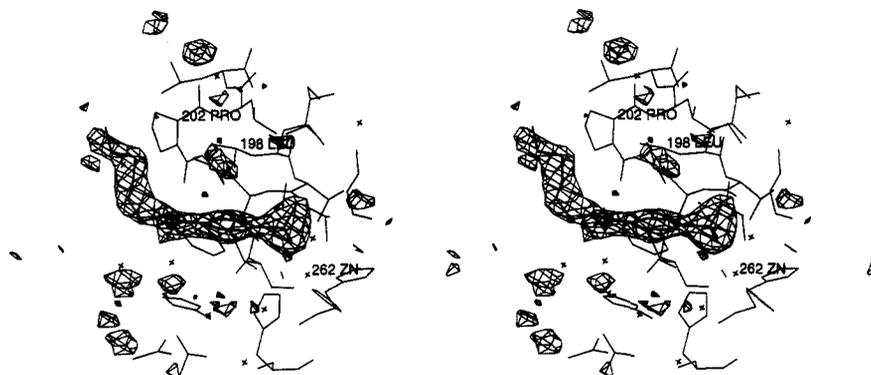
Figure 2. Difference electron density map of the CAII−EG$_3$PheNH$_3^+$ complex calculated with Fourier coefficients $|F_o| - |F_c|$ and phases derived from the final model less the inhibitor. The map is contoured at 2.5σ and refined atomic coordinates are superimposed (only the ordered atoms of the inhibitor are shown); Leu198, Pro202, and zinc are indicated.

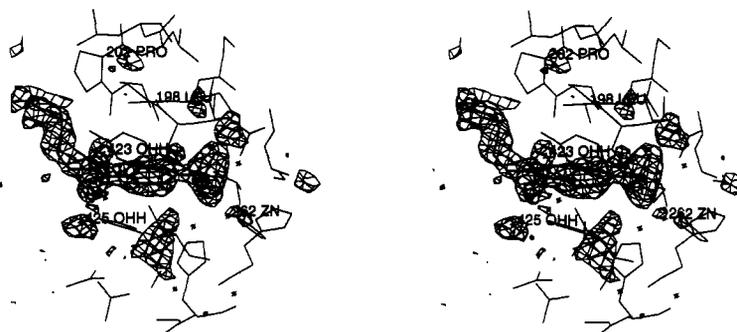**Figure 3.** Difference electron density map of the CAII−EG$_3$GlyNH$_3^+$ complex calculated with Fourier coefficients $|F_o| - |F_c|$ and phases derived from the final model less the inhibitor. The map is contoured at 2.5σ, and refined atomic coordinates are superimposed (only the ordered atoms of the inhibitor are shown); Leu198, Pro202, zinc, and water molecules 423 and 425 (which bridge the enzyme and inhibitor by hydrogen bonds) are indicated.

Figure 4. Difference electron density map of the CAII−EG$_3$NH$_3^+$ complex calculated with Fourier coefficients $|F_o| - |F_c|$ and phases derived from the final model less the inhibitor and water molecules. The map is contoured at 2.0σ and refined atomic coordinates are superimposed (only the ordered atoms of the inhibitor are shown); Leu198, Pro202, zinc, and water molecule 425 are indicated. Electron density corresponding to an alternate, low occupancy, conformation of the poly(ethylene glycol) tail, extending into the hydrophilic region of the active site cavity, is clearly visible.

The van der Waals contact surface areas between CAII and the glycol tails of the inhibitors EG$_3$PheNH$_3^+$, EG$_3$GlyNH$_3^+$, and EG$_3$NH$_3^+$ (only ordered atoms were included in the calculation) are 62, 64, and 61 Å^2, respectively. Interestingly, differences in contact surface area of the poly(ethylene glycol) tails vary less than 8 Å^2; similarly, the contact surface area of the anchoring group of each arylsulfonamide inhibitor remains essentially constant. Since there are no hydrogen bonds between the oxygen atoms of the glycol tail and the enzyme, van der Waals contact surface area must be the principal determinant of enzyme−poly(ethylene glycol) association.

Discussion

The key finding of this study is that variation in the structure of amino acids at locations distant from the primary binding site affects the overall binding affinity of the inhibitor (e.g., K_d (EG$_3$PheNH$_3^+$) = 14 nM vs K_d (EG$_3$GluNH$_3^+$) = 100 nM). Fluorescence measurements demonstrate that poly(ethylene glycol)-based inhibitors with pendant hydrophobic amino acids modestly improve binding, even though the crystal structures of the three inhibitors studied do not reveal ordered electron density for the terminal region of the glycol group. It is conceivable that the ethylene glycol chain might have
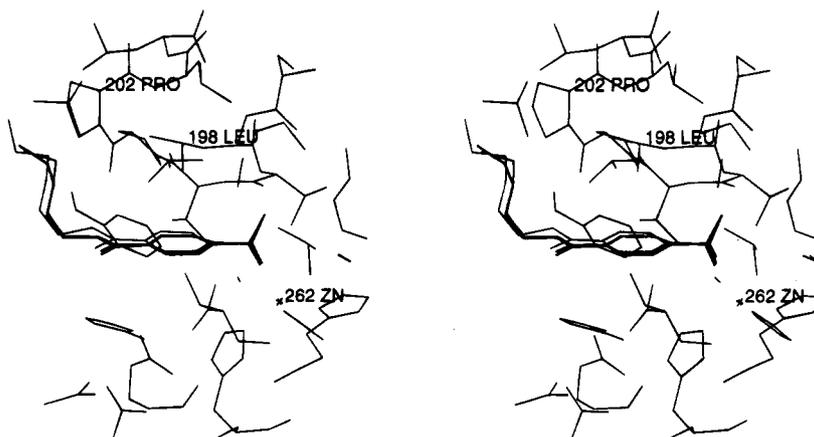
Figure 5. Superposition of the crystallographically observable portions of $EG_3PheNH_3^+$ (thin bonds), $EG_3GlyNH_3^+$ (medium bonds), and $EG_3NH_3^+$ (thick bonds) bound to the active site of CAII. Note that the glycol tails of these inhibitors adopt roughly similar conformations as they associate with the Pro202/Leu198 hydrophobic wall.
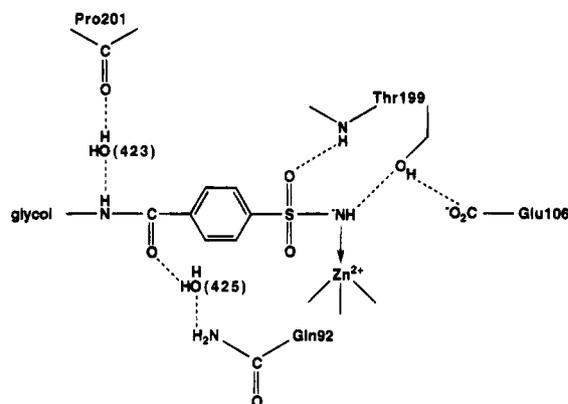

Figure 6. Binding mode of the CAII–$EG_3GlyNH_3^+$ complex. Hydrogen bonds are indicated by dashed lines.

folded back on itself to place the terminal hydrophobic group in the interior of the CAII; this conformation, however, is not observed.

As a molecular linker between the pendant amino acid and the arylsulfonamide in this series of inhibitors, it is not surprising that poly(ethylene glycol) is relatively conformationally mobile. However, it is notable that the $(EG)_n$ group exhibits greater affinity for the CA surface than does $(Gly)_n$ for inhibitors of comparable length. To illustrate, Jain and colleagues[22] report a K_d of 370 nM for a $(Gly)_4$ inhibitor, while $EG_3GlyNH_3^+$ has a K_d of 19 nM. Nevertheless, the conformational freedom of the EG_3 tail (and even a Gly_n tail) increases the entropic cost of enzyme–inhibitor association, and a substantial entropic price must be paid in order to optimize its contact with the enzyme. Accordingly, these terminally unsubstituted inhibitors containing $(EG)_n$ or $(Gly)_n$ groups bind at best only ∼100-fold better than the unsubstituted arylsulfonamide (K_d = 1540 nM).[24]

The association of the poly(ethylene glycol) tail to the hydrophobic region of the active site may restrict the possible binding modes of the terminal amino acid. While altering the length of the poly(ethylene glycol) tail may increase the possible binding modes of a pendant amino acid, this increase seems not to lower the dissociation constant, in part, we assume, because of compensatory entropic terms. Interestingly, the ethylene glycol chain approximately follows the same path as does the $(Gly)_n$ chain of the inhibitors bearing that group.[21] This common binding mode may be due in part to the steering effect of the benzamide group,

which apparently directs the linker chain primarily toward the hydrophobic side of the active site cleft. Work is currently underway to develop an inhibitor that will interact with the hydrophilic region of the active site.

Experimental Section

Materials and Methods. All reactions were monitored by thin-layer chromatography (TLC) using 0.25-mm precoated silica gel plates (E. Merck). Column chromatography was preformed with the indicated solvents using silica gel 60 (particle size 0.040–0.063 mm) supplied by E. Merck. Carbon and proton NMR spectra were measured on either a Bruker AM-500 MHz or AM-400 MHz spectrometer as indicated. Chemical shifts are reported relative to internal tetramethylsilane in $CDCl_3$ samples; in CD_3OD the solvent peak is set to 4.79 ppm, and in DMSO-d_6 the solvent peak is set to 2.49 ppm. Fluorescence measurements were made on a Perkin-Elmer Model MPF-4 spectrofluorimeter, equipped with a water bath to regulate temperature.

The 2,2′-(ethylenedioxy)diethylamine and 4-sulfamoylbenzoic acid were obtained from Fluka; the protected amino acids were purchased from Bachem Biosciences, Inc. Reaction conditions have not been optimized.

Abbreviations: DMF, dimethylformamide; TFA, trifluoroacetic acid; Boc, *tert*-butyloxycarbonyl; EDC, 1-[3-(dimethylamino)propyl]-3-ethylcarbodiimide hydrochloride; HOBT, 1-hydroxybenzotriazole.

EG_3NHBoc: $H_2NO_2SC_6H_4CONH(CH_2CH_2O)_2CH_2CH_2$-$NHCO_2CH_2NHCO_2C(CH_3)_3$. 4-Sulfamoylbenzoic *N*-hydroxysuccinimide ester (298 mg, 1 mmol) and 2,2′-(ethylenedioxy)-diethylamine mono-*tert*-butyl carbamate (248 mg, 1 mmol) were dissolved in DMF (6 mL) at room temperature. The solution was stirred for 18 h, and then the DMF was removed *in vacuo*. The residue was taken up in ethyl acetate (5 mL), poured into a 5% solution of sodium bicarbonate (5 mL), and extracted with ethyl acetate. The combined organic layers were dried over sodium sulfate and filtered, and the solvent was removed *in vacuo*. Flash chromatography (90% ethyl acetate/7% hexanes/3% methanol) gave the *tert*-butyl carbamate of $EG_3NH_3^+$ (420 mg) as a colorless solid: mp 129.5–130.5 °C; ^{1}H NMR (500 MHz, DMSO-d_6) δ 1.35 (s, 9H), 3.04 (dd, J = 5.9, 11.9 Hz, 2 H), 3.32–3.37 (comp m, 6 H), 3.42 (dd, J = 5.8, 11.5 Hz, 2 H), 6.76 (t, J = 5.3 Hz, 1 H), 7.46 (s, 2 H), 7.87 (d, J = 8.2 Hz, 2H), 7.97 (d, J = 8.4 Hz, 2 H), 8.70 (t, J = 5.5 Hz, 1 H); ^{13}C NMR (100 MHz, DMSO-d_6) δ 30.1, 68.8, 69.1, 69.4, 77.6, 125.6, 127.8, 137.2, 146.2, 155.5, 165.2; high-resolution mass spectrum (FAB) m/z 454.1637 [(M + Na)$^+$; calcd for $C_{18}H_{29}O_7N_3SNa$ 454.1624].

$EG_3NH_3^+$ (3): $H_2NO_2SC_6H_4CONH(CH_2CH_2O)_2CH_2CH_2$-$NH_3^+$·TFA. Boc-protected **3** (312 mg, 0.72 mmol) was dissolved in TFA (4.8 mL) to 0 °C and stirred for 8 min. The acid was removed *in vacuo*, and the residue was taken up in

Table 3. Data Collection and Refinement Statistics for Carbonic Anhydrase II−Inhibitor Complexes

inhibitor	EG$_3$PheNH$_3^+$	EG$_3$GlyNH$_3^+$	EG$_3$NH$_3^+$
number of crystals	3	1	1
number of measured reflections	18135	24258	34958
number of unique reflections	10064	12645	11205
maximum resolution (Å)	2.3	2.0	1.9
R_{merge}[a]	0.060	0.080	0.089
number of water molecules in final cycle of refinement	76	78	88
number of reflections used in refinement (6.5−max. resolution, Å)	9389	11946	10446
R factor[b]	0.180	0.174	0.174
RMS deviation from ideal bond lengths (Å)	0.013	0.013	0.011
RMS deviation from ideal bond angles (deg)	1.9	1.9	1.8
RMS deviation from ideal planarity (Å)	0.009	0.011	0.010
RMS deviation from ideal chirality (Å^3)	0.105	0.104	0.111

[a] R_{merge} for replicate reflections, $R = \Sigma|I_{hi} - <I_h>|/\Sigma<I_h>$; I_{hi} = intensity measured for reflection h in data set i, $<I_h>$ = average intensity for reflection h calculated from replicate data. [b] Crystallographic R factor, $R = \Sigma||F_o| - |F_c||/\Sigma|F_o|$; $|F_o|$ and $|F_c|$ are the observed and calculated structure factors, respectively.

water and concentrated to remove traces of acid, furnishing EG$_3$NH$_3^+$ (335 mg) as a thick syrup: ^{1}H NMR (400 MHz, DMSO-d_6) δ 2.96 (m, 2 H), 3.45 (dd, J = 5.8, 11.6 Hz, 2 H), 3.54−3.60 (comp m, 8 H), 7.50 (s, 2 H), 7.79 (s, 1 H), 7.90 (d, J = 8.5 Hz, 2 H), 7.99 (d, J = 1.9, 6.7 Hz, 2 H), 8.74 (t, J = 5.5 Hz, 1 H); ^{13}C NMR (100 MHz, DMSO-d_6) δ 66.7, 68.8, 69.4, 69.7, 125.6, 127.9, 137.2, 146.3, 165.3; high-resolution mass spectrum (FAB) m/z 332.1289 [(M + H)$^+$; calcd for C$_{13}$H$_{22}$O$_5$N$_3$S 332.1280].

EG$_3$GlyBoc: H$_2$NO$_2$SC$_6$H$_4$CONH(CH$_2$CH$_2$O)$_2$CH$_2$CH$_2$-NHCO$_2$CH$_2$NHCO$_2$C(CH$_3$)$_3$. Amine salt 3 (100 mg, 0.22 mmol) was dissolved in acetonitrile (1 mL) containing triethylamine (50 mL, 0.34 mmol). Boc-glycine-N-hydroxysuccinamide ester (122 mg, 0.45 mmol) was added at room temperature. White precipitate formed at 3 min. CHCl$_3$ (3 mL) was added to aid stirring, but most of the precipitate remained. After 3 h, the solvent was removed *in vacuo*. The residue was taken up in CH$_2$Cl$_2$ and washed with water (a slight emulsion formed). The organic portion was dried over sodium sulfate; after decanting, the solvent was removed *in vacuo* and the residue was purified by flash chromatography (5% MeOH/ 94.5% CH$_2$Cl$_2$/0.5% AcOH) to give 33 mg of the *tert*-butyl carbamate of EG$_3$GlyBoc as a white powder: mp 149−150 °C; ^{1}H NMR (400 MHz, CD$_3$OD) δ 1.32 (s, 9 H), 3.24 (m, 2 H), 3.47 (m, 2 H), 3.51−3.56 (comp m, 8 H), 7.86 (s, 4 H); ^{13}C NMR (100 MHz, CD$_3$OD) δ 28.7, 40.3, 41.1, 44.7, 70.5, 70.6, 71.4, 80.8, 127.4, 129.1, 139.1, 147.8, 169.0, 172.6; high-resolution mass spectrum (FAB) m/z 489.2028 [(M + H)$^+$; calcd for C$_{20}$H$_{33}$O$_8$N$_4$S 489.2019].

EG$_3$PheBoc: H$_2$NO$_2$SC$_6$H$_4$CONH(CH$_2$CH$_2$O)$_2$CH$_2$CH$_2$-NHCO$_2$CH$_2$(CH$_2$C$_6$H$_5$)NHCO$_2$C(CH$_3$)$_3$. Amine salt 3 (100 mg, 0.22 mmol) was dissolved in acetonitrile (1 mL) containing triethylamine (50 μL, 0.34 mmol). Boc-phenylalanine (120 mg, 0.44 mmol), HOBT (66 mg, 0.44 mmol), and EDC (86 mg, 0.44 mmol) were added sequentially to the amine at room temperature. After the mixture was stirred for 4.5 h, the solvent was removed *in vacuo* and the residue was taken up in CH$_2$Cl$_2$. The organic solution was washed in succession with 5% bicarbonate solution and saturated ammonium chloride solution and dried over sodium sulfate. After filtration, the solvent was removed *in vacuo* and the residue was purified by flash chromatograph (5% MeOH/94.5% CH$_2$Cl$_2$/0.5% AcOH) to give 130 mg of EG$_3$PheBoc as a white powder: mp 135.5−136.5 °C; ^{1}H NMR (500 MHz, CDCl$_3$ + 10% CD$_3$OD) δ 1.37 (s, 9 H), 2.90 (dd, J = 7.5, 13.1 Hz, 1 H), 3.03 (dd, J = 6.7, 13.2 Hz, 1 H), 3.28−3.36 (comp m, 3 H), 3.46 (d, J = 4.5 Hz, 1 H), 3.55− 3.64 (comp m, 6 H), 3.67 (m, 2 H), 4.28 (t, J = 6.7 Hz, 1 H), 7.20 (m, 3 H), 7.27 (t, J = 7.2 Hz, 2 H), 7.94 (dd, J = 8.4, 17.4, Hz, 4 H); ^{13}C NMR (100 MHz, CDCl$_3$ + 10% CD$_3$OD) δ 27.7, 38.4, 38.7, 39.5, 55.4, 69.0, 69.2, 69.7, 77.8, 125.9, 126.4, 127.5, 128.1, 128.9, 129.0, 136.4, 137.3, 145.2, 155.5, 166.8, 171.9; high-resolution mass spectrum (FAB) m/z 601.2314 [(M + Na)$^+$; calcd for C$_{27}$H$_{38}$O$_8$N$_4$SNa 601.2308].

EG$_3$GlyNH$_3^+$ (2): H$_2$NO$_2$SC$_6$H$_4$CONH(CH$_2$CH$_2$O)$_2$CH$_2$-CH$_2$NHCOCH$_2$NH$_3^+$·TFA. EG$_3$-Gly-Boc (21 mg, 0.043 mmol) was dissolved in CH$_2$Cl$_2$ (200 mL) and TFA (200 mL), and the

mixture was stirred for 30 min at room temperature. The solvent was removed *in vacuo* and the residue concentrated from water twice to remove excess TFA to give the amine salt as a colorless syrup (20 mg): ^{1}H NMR (500 MHz, CD$_3$OD) d 3.27 (t, J = 5.3 Hz, 2 H), 3.43 (t, J = 5.4 Hz, 2 H), 3.46−3.57 (comp m, 10 H), 7.85 (m, 4 H); ^{13}C NMR (100 MHz, CD$_3$OD) δ 40.5, 41.0, 41.5, 70.4, 70.5, 71.4, 127.3, 129.0, 139.0, 147.7, 167.3, 169.0; high-resolution mass spectrum (FAB) m/z 389.1487 [M$^+$; calcd for C$_{15}$H$_{25}$O$_6$N$_4$S 389.1493].

EG$_3$PheNH$_3^+$ (1): H$_2$NO$_2$SC$_6$H$_4$CONH(CH$_2$CH$_2$O)$_2$CH$_2$-CH$_2$NHCOCH(CH$_2$C$_6$H$_5$)NH$_3^+$·TFA. EG$_3$PheBoc (45 mg, 0.078 mmol) was dissolved in CH$_2$Cl$_2$ (400 mL) and TFA (400 mL), and the mixture was stirred for 30 min at room temperature. The solvent was removed *in vacuo* and the residue concentrated from water twice to remove excess TFA. EG$_3$-PheNH$_3^+$ was obtained as a colorless syrup (44 mg): ^{1}H NMR (500 MHz, CD$_3$OD) δ 2.92 (dd, J = 7.4, 13.8 Hz, 1 H), 3.01 (dd, J = 7.1, 13.7 Hz, 1 H), 3.12−3.27 (comp m, 3 H), 3.33 (m, 1 H), 3.43 (m, 4 H), 3.51 (m, 4 H), 3.91 (t, J = 7.3 Hz, 1 H), 7.12 (m, 2 H), 7.15 (m, 1 H), 7.20 (m, 1 H), 7.82 (m, 4 H); ^{13}C NMR (100 MHz, CD$_3$OD) δ 38.7, 40.5, 41.0, 55.8, 70.3, 70.5, 71.3, 71.4, 127.4, 128.9, 129.1, 130.1, 130.6, 135.7, 139.0, 147.7, 169.0, 169.6; high-resolution mass spectrum (FAB) m/z 479.1977 [M$^+$; calcd for C$_{22}$H$_{31}$O$_6$N$_4$S 479.1962].

Crystallography. Native blood CAII was purchased from Sigma and used without further purification. Typical enzyme− inhibitor cocrystallizations, performed using the sitting drop method, required the addition of a 5-μL drop containing 0.3 mM enzyme, 50 mM Tris-HCl (pH 8.0 at room temperature), 150 mM NaCl, 3 mM NaN$_3$, and inhibitor [4.3 mM 1 or 3 dissolved in methanol, or 4.1 mM 2 dissolved in DMSO, such that the final concentration of organic solvent in the crystallization well was 5% (vol/vol)] to a 5-μL drop containing 50 mM Tris-HCl (pH 8.0 at room temperature), 150 mM NaCl, and 3 mM NaN$_3$ with 1.75−2.5 M ammonium sulfate in the crystallization well. For the CAII−2 complex it was necessary to add 0.1 mM β-octylglucoside[25] to the crystallization buffer in order to facilitate crystal growth.

For each crystallization trial, precipitant and enzyme drops were saturated with methylmercury acetate in order to promote the growth of diffraction quality parallelepipedons.[26] Crystals typically appeared within 2 weeks at 4 °C. Each enzyme−inhibitor complex crystallized isomorphously with the native enzyme (space group $P2_1$, unit cell parameters a = 42.7 Å, b = 41.7 Å, c = 73.0 Å, and β = 104.6°. Crystals were harvested and mounted and sealed in either 0.5 or 0.7 mm glass capillaries with a small portion of mother liquor.

A Siemens X-100A multiwire area detector, mounted on a three-axis camera and equipped with a Charles Supper double X-ray focusing mirrors, was used for X-ray collection. A Rigaku RU-200 rotating anode X-ray generator operating at 45 kV/55 mA supplied Cu Kα radiation. All data were collected at room temperature by the oscillation method; for each experiment, the crystal-to-detector distance was set at either 10 or 12 cm and the detector swing angle was set to either 20 or 22°. Data frames of 0.083 33° oscillation about ω

were collected, with exposure times of 60 s per frame, for total angular rotation ranges about ω of at least 74° per experiment. Raw data frames were analyzed using BUDDHA,[27] reflections with $I < 2\sigma$ were discarded, and replicate and symmetry-related structure factors were merged using PROTEIN;[28] relevant data collection and reduction statistics are recorded in Table 3.

In the structure determination of each CAII–inhibitor complex, structure factors obtained from the corrected intensity data were used to generate difference electron density maps using Fourier coefficients $|F_o| - |F_c|$ or $2|F_o| - |F_c|$ with phases calculated from the structure of refined human CAII;[14,15] atomic coordinates were obtained from the Brookhaven Protein Data Bank.[29] Inspection of the electron density maps revealed that only minor adjustments to the protein model were required, and model building was performed with the graphics software FRODO[30] installed on an Evans and Sutherland PS390 interfaced with a VAXstation 3500. Atomic coordinates were then refined against the observed data with PROLSQ.[31] Neither the inhibitor atoms nor the active site water molecules were included in the initial stages of refinement for each enzyme–inhibitor complex. Residue conformations throughout the protein were examined and adjusted during the course of refinement using maps generated with Fourier coefficients outlined above and phases calculated from the in-progress atomic model.

During the refinement of each CAII–inhibitor complex, inhibitor atoms and active site solvent molecules were added when the crystallographic R factor dropped below 0.200. Solvent molecules were deleted from the model if their thermal B factors rose above 50 Å² during the course of refinement. We note that for each bound inhibitor, a portion of its glycol "tail" was not observed in electron density maps (presumably due to molecular disorder); therefore, the occupancies of all unobserved atoms in the poly(ethylene glycol) tails were set to zero in final atomic coordinate sets. The refinement of each enzyme–inhibitor complex converged smoothly to final crystallographic R factors within the range 0.174–0.180. Each final model exhibited good stereochemistry with rms deviations from ideal bond lengths and bond angles ranging from 0.011 to 0.013 Å and from 1.8 to 1.9°, respectively. Pertinent refinement statistics are recorded in Table 3, and the coordinates of each enzyme–inhibitor complex have been deposited into the Brookhaven Protein Data Bank.[29]

References

(1) Coleman, J. E. Chemical Reactions of Sulfonamides with Carbonic Anhydrase. *Annu. Rev. Pharmacol.* **1975**, *15*, 221–242.
(2) Lindskog, S. The Structural Basis of Kinetic Differences between Carbonic Anhydrase Isoenzymes. In *Zinc Enzymes*; Bertini, I., Luchinat, C., Maret, W., Zeppezauer, M., Eds.; Birkhauser: Boston, 1986; pp 307–316.
(3) Silverman, D. N.; Lindskog, S. The Catalytic Mechanism of Carbonic Anhydrase: Implications of a Rate-Limiting Protolysis of Water. *Acc. Chem. Res.* **1988**, *21*, 30–36.
(4) Christianson, D. W. Structural Biology of Zinc. *Adv. Protein Chem.* **1991**, *42*, 281–355.
(5) Kinsey, V. E. Comparative Chemistry of Aqueous Humor in Posterior and Anterior Chambers of Rabbit Eye. *Arch. Ophthamol.* **1953**, *50*, 401–417.
(6) Friedenwald, J. S. The Formation of the Intraocular Fluid. *Am. J. Ophthamol.* **1949**, *32*, 9–27.
(7) Mann, T.; Keilin, D. Sulphanilamide as a Specific Inhibitor of Carbonic Anhydrase. *Nature* **1940**, *146*, 164–165.
(8) Becker, B. Decrease in Intraocular Pressure in Man by a Carbonic Anhydrase Inhibitor, Diamox. *Am. J. Ophthamol.* **1954**, *37*, 13–15.
(9) Grant, W. M.; Trotter, R. R. Diamox (Acetazolamide) in Treatment of Glaucoma. *Arch. Ophthamol.* **1954**, *51*, 735–739.
(10) Breinin, G. M.; Görtz, H. Carbonic Anhydrase Inhibitor Acetazolamide (Diamox). *Arch. Ophthamol.* **1954**, *52*, 333–348.
(11) Maren, T. H. Carbonic Anhydrase: General Perspectives and Advances in Glaucoma Research. *Drug Dev. Res.* **1987**, *10*, 255–276.

(12) Maren, T. H. The Links Among Biochemistry, Physiology, and Pharmacology in Carbonic Anhydrase Mediated Systems. In *Carbonic Anhydrase: From Biochemistry and Genetics to Physiology and Clinical Medicine*; Botrè, F., Gros, G., Storey, B. T., Eds.; VCH Publishers: New York, 1991; pp 186–207.
(13) Maren, T. H. Direct Measurements of the Rate Constants of Sulfonamides with Carbonic Anhydrase. *Mol. Pharmacol.* **1992**, *41*, 419–426.
(14) Eriksson, A. E.; Jones, T. A.; Liljas, A. Crystallographic Studies of Human Carbonic Anhydrase II (HCAII). In *Zinc Enzymes*; Bertini, I., Luchinat, C.; Maret, W., Zeppezauer, M., Eds.; Birkhauser: Boston, 1986; pp 317–328.
(15) Eriksson, A. E.; Jones, T. A.; Liljas, A. Refined Structure of Human Carbonic Anhydrase II at 2.0 Å Resolution. *Proteins: Struct. Funct. Gen.* **1988**, *4*, 274–282.
(16) Håkansson, K.; Carlsson, M.; Svensson, L. A.; and Liljas, A. Structure of Native and Apo Carbonic Anhydrase II and Structure of Some of Its Anion-Ligand Complexes. *J. Mol. Biol.* **1992**, *227*, 1192–1204.
(17) Eriksson, A. E.; Kylsten, P. M.; Jones, T. A.; Liljas, A. Crystallographic Studies of Inhibitor Binding Sites in Human Carbonic Anhydrase II: A Pentacoordinated Binding of the SCN⁻ Ion to the Zinc at High pH. *Proteins: Struct. Funct. Gen.* **1988**, *4*, 283–293.
(18) Baldwin, J. J.; Ponticello, G. S.; Anderson, P. S.; Christy, M. E.; Murcko, M. A.; Randall, W. C.; Schwam, H.; Sugrue, M. F.; Springer, J. P.; Gautheron, P.; Grove, J.; Mallorga, P.; Viader, M.; McKeever, B. M.; Navia, M. A. Thienothiopyran-2-sulfonamides: Novel Topically Active Carbonic Anhydrase Inhibitors for the Treatment of Glaucoma. *J. Med. Chem.* **1989**, *32*, 2510–2513.
(19) Vidgren, J.; Liljas, A.; Walker, N. P. C. Refined Structure of the Acetazolamide Complex of Human Carbonic Anhydrase II at 1.9 Å. *Int. J. Biol. Macromol.* **1990**, *12*, 342–344.
(20) Prugh, J. D.; Hartman, G. D.; Mallorga, P. J.; McKeever, B. M.; Michelson, S. R.; Murcko, M. A.; Schwam, H.; Smith, R. L.; Sondey, J. M.; Springer, J. P.; Sugrue, M. F. New Isomeric Classes of Topically Active Ocular Hypotensive Carbonic Anhydrase Inhibitors: 5-Substituted Thieno[2,3-b]thiophene-2-sulfonamides and 5-Substituted Thieno[3,2-b]thiophene-2-sulfonamides. *J. Med. Chem.* **1991**, *34*, 1805–1818.
(21) Bunn, A. M. C.; Alexander, R. S.; Christianson, D. W. Mapping Protein-Peptide Affinity: Binding of Peptidylsulfonamide Inhibitors to Human Carbonic Anhydrase II. *J. Am. Chem. Soc.* **1994**, *116*, 5063–5068.
(22) Jain, A.; Huang, S. G.; Whitesides, G. M. Lack of Effect of the Length of Oligoglycine- and Oligo(ethylene glycol)-Derived para-Substituents on the Affinity of Benzenesulfonamides for Carbonic Anhydrase II in Solution. *J. Am. Chem. Soc.* **1994**, *116*, 5057–5062.
(23) Chen, R. F.; Kernohan, J. C. Combination of Bovine Carbonic Anhydrase with a Fluorescent Sulfonamide. *J. Biol. Chem.* **1967**, *242*, 5813–5823.
(24) Taylor, P. W.; King, R. W.; Burgen, A. S. V. Kinetics of Complex Formation Between Human Carbonic Anhydrases and Aromatic Sulfonamides. *Biochemistry* **1970**, *9*, 2638–2645.
(25) McPherson, A.; Koszelak, S.; Axelrod, H.; Day, J.; Williams, R.; Robinson, L.; McGrath, M.; Cascio, D. An Experiment Regarding Crystallization of Soluble Proteins in the Presence of β-Octyl Glucoside. *J. Biol. Chem.* **1986**, *261*, 1969–1975.
(26) Tilander, B.; Strandberg, B.; Fridborg, K. Crystal Structure Studies on Human Erythrocyte Carbonic Anhydrase C (II). *J. Mol. Biol.* **1965**, *12*, 740–760.
(27) Durbin, R. M.; Burns, R.; Moulai, J.; Metcalf, P.; Freymann, D.; Blum, M.; Anderson, J. E.; Harrisson, S. C.; Wiley, D. C. Protein, DNA, and Virus Crystallography with a Focused Imaging Proportional Counter. *Science* **1986**, *232*, 1127–1132.
(28) Steigemann, W. Die Entwicklung und Anwendung von Rechenverfahren und Rechenprogrammen zur Strukturanalyse von Proteinem am Beispiel des trypsin-trypsinihibitor Komplexes, des freien Inhibitors und der L-Asparaginase. Ph.D. Thesis, Max Plank Institut für Biochemie, 1974.
(29) Bernstein, F. C.; Koetzle, T. F.; Williams, G. J. B.; Meyer, E. F., Jr.; Brice, M. D.; Rodgers, J. R.; Kennard, O.; Shimanouchi, T.; Tasumi, M. The Protein Data Bank: A Computer-based Archival File for Macromolecular Structures. *J. Mol. Biol.* **1977**, *112*, 535–542.
(30) Jones, T. A. Interactive Computer Graphics: FRODO. *Methods Enzymol.* **1985**, *115*, 157–171.
(31) Hendrickson, W. A. Stereochemically Restrained Refinement of Macromolecular Structures. *Methods Enzymol.* **1985**, *115*, 252–270.